CrystEngComm

Cite this: *CrystEngComm*, 2012, **14**, 2251

www.rsc.org/crystengcomm

PAPER

Template-free synthesis of mesoporous $NaTbF_4$ and $NaTbF_4$:Eu nano-rice and their luminescence properties†

Zhiming Chen,[ab] Zhirong Geng,[a] Dalin Shao,[a] Zhiping Zhou[a] and Zhilin Wang*[a]

Received 17th July 2011, Accepted 5th December 2011
DOI: 10.1039/c2ce05909f

Single-crystalline mesoporous $NaTbF_4$ nano-rice have been successfully synthesized in large scale by reaction of aqueous Tb^{3+} with sodium fluoride in the presence of ethylenediaminetetraacetic acid (EDTA) at 110 °C for 12 h, which were confirmed by X-ray powder diffraction, energy dispersive X-ray analysis, transmission electron microscopy, scanning electron microscopy, and nitrogen adsorption–desorption isotherms. A mechanism for the formation of the mesoporous nano-rice by an EDTA-directed assembly process accompanied by the localized Ostwald ripening has been proposed based on the observations of time-dependent experiments. In addition, this novel nano-rice can be used as an excellent host lattice for Eu^{3+} ions, in which the luminescence properties of Eu^{3+} would be improved significantly. Our study indicates that the maximum quantum efficiency of $NaTbF_4$:Eu nano-rice reaches up to 69.9%. This work demonstrates that morphology-controlled synthesis can offer a simple solution to fabricate mesoporous $NaTbF_4$:Eu nano-rice for technological and biomedical applications.

Introduction

In modern chemistry and materials science, the precise architectural manipulation of inorganic functional materials with well-defined morphologies and accurately tunable sizes has been a research hotspot and a challenging issue because it is well known that the properties of the materials closely interrelate with geometrical factors such as shape, dimensionality, and size.[1–5] So, many efforts have been devoted to explore excellent synthetic approaches for the fabrication of different kinds of inorganic nanocrystals with distinct structural and geometrical features. Thus far, a wide variety of functional materials, including metal oxide,[6,7] sulfide,[8,9] hydrate,[10] fluoride,[11–13] and other minerals,[14,15] have been successfully prepared with hierarchical structures, in which those that possess porous structures received special attention because they provide opportunities for exploiting novel properties due to their high surface-to-volume ratio and permeability. Therefore, the synthesis of mesoporous materials represents a remarkable level in current chemistry and materials science. Generally, the materials of ordered mesopores are synthesized through a soft or hard template formation process.[6,10,15–41] However, the use of templates usually suffers from disadvantages related to high cost and tedious synthetic procedures, which may prevent them from being used in large-scale applications.[9] Therefore, the development of template-free syntheses is seriously considered.

As an important category of functional materials, rare earth based compounds have drawn continuous research attention for many years not only for fundamental scientific interest but also for their various applications in fields such as optics,[42–44] MALDI matrix,[45] biological labeling and imaging,[46–49] and catalysis.[50] This is because these useful functions mainly originate from the electron transitions within the 4f shell, and are highly sensitive to the composition and structures of the rare earth compounds, especially to the complexation state and the crystal field of the matrix in which rare earth ions are trapped.[51,52] Materials with lower phonon energy are required as the luminescent host to minimize non-radiative loss. Rare earth fluorides such as $NaLnF_4$ and LnF_3, possessing a high refractive index and low phonon energies, can be regarded as excellent host lattices for lanthanide ions.[53–55] Recent attempts to introduce rare earth ions into well-defined porous nanostructures can enhance their optical properties, indicating that energy can be transferred to rare-earth ions more effectively in this way.[56,57] Therefore, it still remains a great challenge to develop facile one-step, template-free methods for the preparation of rare earth fluoride crystals with well-defined porous structures.

Herein, we present a one-pot template-free hydrothermal process for the synthesis of mesoporous $NaTbF_4$ nano-rice by reaction of aqueous Tb^{3+} with sodium fluoride in the presence of EDTA. The structure, formation mechanism, and luminescence properties of the products were investigated in detail. When Eu^{3+} ions (2%) were introduced into these mesoporous nano-rice, the

[a]*State Key Laboratory of Coordination Chemistry, School of Chemistry and Chemical Engineering, Nanjing University, Nanjing, 210093, People's Republic of China. E-mail: wangzl@nju.edu.cn; Fax: +86-25-83317761; Tel: +86-25-83686082*
[b]*Department of Biochemical Engineering, Anhui Polytechnic University, Wuhu, 241000, People's Republic of China*

† Electronic supplementary information (ESI) available: XRD patterns for $NaTbF_4$ and $NaTbF_4$:Eu nano-rice, SEM images mesoporous $NaTbF_4$:Eu nano-rice, FT-IR spectrum of $NaTbF_4$ products, EDX spectra of $NaTbF_4$:Eu nano-rice. See DOI: 10.1039/c2ce05909f

high quantum efficiency (69.9%) and long lifetime (6.97 ms) of the $^5D_0$ lever of Eu^{3+} favour the optical properties of these mesoporous materials. This work not only gives new insight into the fabrication of mesoporous architectures but also sheds some light on the enhancement of luminescence properties, which may provide promising applications.

Results and discussion

The synthesis of mesoporous $NaTbF_4$ nano-rice has been achieved in a water/ethanol solution containing $Tb(NO_3)_3$ and NaF by thermal treatment in the presence of EDTA for 12 h. Fig. 1a shows the XRD pattern of the as-prepared sample. All the positions of the peaks can be readily indexed to hexagonal $NaTbF_4$ phase according to JCPDS file No. 27-0809, indicating the high purity of our products. Well-resolved diffraction peaks reveal good crystallinity of the $NaTbF_4$ specimens. Further evidence of the composition of $NaTbF_4$ came from EDX analysis. It is clear that the sample is composed of only Na, Tb and F, and the atomic ratio for Na/Tb/F is near 1/1/4, in agreement with the expected stoichiometry of the $NaTbF_4$ phase (Fig. 1b).

The morphology of the as-obtained $NaTbF_4$ product was visualized by TEM and SEM measurements. Fig. 2a shows a typical SEM image of the product and reveals that the sample is in the form of a rice-grain like architecture with an average width of 110∼135 nm and length of 210∼260 nm. TEM observations confirmed the result of the SEM measurements. Fig. 2b reveals that these nano-rice exhibit an obvious porous structure, and the contained nanopores are approximately 3∼5 nm in diameter.

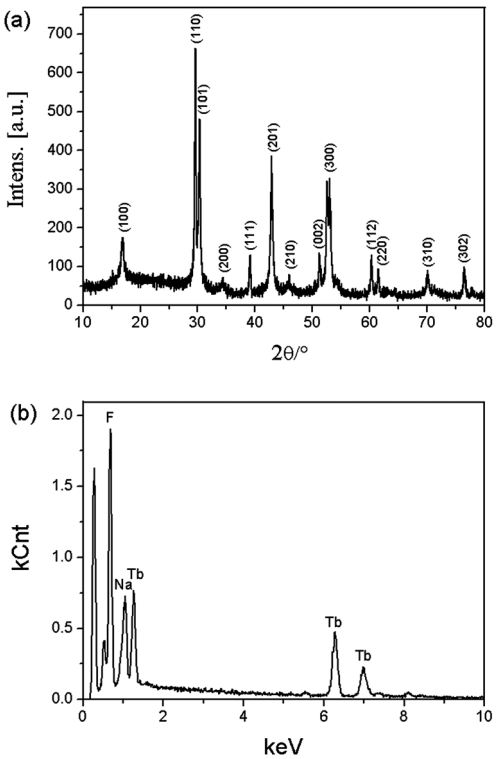

Fig. 1 (a) XRD pattern and (b) EDX analysis of $NaTbF_4$ nano-rice obtained by the reaction of Tb^{3+} with NaF in the presence of EDTA for 12 h.

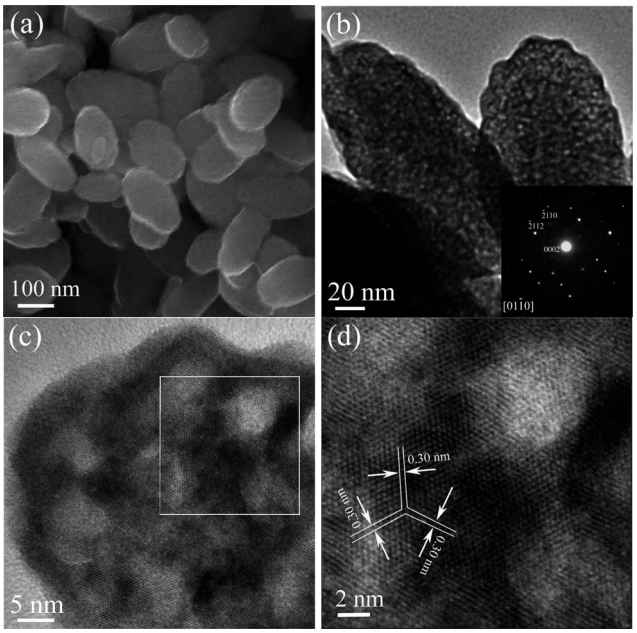

Fig. 2 (a) SEM image and (b) TEM image of mesoporous $NaTbF_4$ nano-rice, (c) HRTEM image of mesoporous $NaTbF_4$ nano-rice, and (d) the magnified image of the selected area of (c). The inset in (b) shows the single-crystalline SAED pattern of the mesoporous nano-rice.

The corresponding selected-area electron diffraction (SAED) taken from one of the mesoporous $NaTbF_4$ nano-rice indicates that it has a well-defined single-crystalline structure (inset of Fig. 2b). The SAED pattern is along the [01$\bar{1}$0] zone axis, and suggesting that the growth along [0001] directions was confined. It seems that it grew preferentially along the direction of the ($\bar{2}$110) crystal plane. The HRTEM images further reveal the single-crystal characteristic structure of $NaTbF_4$ nano-rice (Fig. 2c and d). The 0.30 nm spacing of crystallographic planes corresponds to the {11$\bar{2}$0} lattice fringe of $NaTbF_4$.

In order to understand the porous structure of $NaTbF_4$ nano-rice, full nitrogen sorption isotherms were measured to gain the information about the nature of the porosity. As shown in Fig. 3, the nitrogen adsorption and desorption isotherms are characteristic of a type IV isotherm with a type H3 hysteresis loop,[58,59]

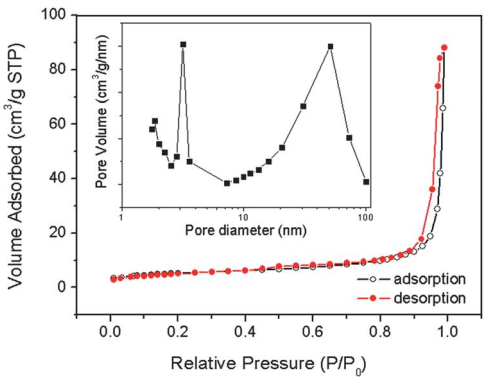

Fig. 3 Typical N_2 gas adsorption–desorption isotherm of rice-grain like $NaTbF_4$ architectures; the inset is the corresponding pore-size distribution.

indicating the presence of mesopores in the size range of 2∼50 nm. Furthermore, the observed hysteresis loop shifts to a higher relative pressure on approaching $P/P_0 \approx 1$, which suggests that macropores (size >50 nm) are also present.[58,59] This hypothesis has been confirmed by the corresponding BJH pore size distribution curve. The BJH analyses show that it also exhibits a bimodal mesopore distribution with sizes of 3.1 and 51 nm. Considering the morphology of the rice-grain like architectures observed in Fig. 2, the smaller pores (∼3.1 nm) may correspond to the pores inside the nano-rice, while the larger pores (∼51 nm) can be attributed to the aggregation of the nano-rice. It is these bimodal mesopores that will endow the as-prepared nano-rice with novel application potentials.

To investigate the formation mechanism of mesoporous $NaTbF_4$ nano-rice, we studied the effect of reaction time and molar ratio of EDTA to Tb^{3+} on the size and morphology of the products. Fig. 4 is a series of TEM images of the samples showing the morphological evolution of the mesoporous nano-rice. When the sample was prepared by 0.5 h heat treatment, primary particles and some rice-grain like aggregates with a width of about 80 nm and lengths of about 245 nm coexisted. The corresponding XRD result confirmed the formation of pure $NaTbF_4$ crystals, and the intensive diffraction peaks reveals the high crystallization of the products (see Fig. S1, ESI†). After 1 h hydrothermal treatment, rice-grain like aggregates with widths of about 70 nm and lengths of about 180 nm (a few were 110 nm in width and 230 nm in length) were obtained. If the reaction time was prolonged to 2 or 6 h, rice-grain like architectures with a larger size were obtained. The corresponding width is about 100 and 120 nm, respectively, and the length increases from 180 to 220 nm. Meanwhile, the intensities of the diffraction peaks of $NaTbF_4$ nano-rice increase significantly, indicating the enhancement of crystallization of the nano-rices.

EDTA is an efficient chelator for rare earth ions. It reacts with Ln^{3+} to form stable Ln-EDTA (1 : 1) complexes. The presence of EDTA is found to be helpful for the formation of several types of rare earth based compounds, such as $NaLnF_4$ nanocrystals,[60] $NaYF_4$:Yb,Er nanocrystals,[46] EuF_3 and SmF_3 microcrystals.[45,61,62] To investigate the effect of EDTA on the morphology of $NaTbF_4$ nanocrystals in our synthetic method, the amount of EDTA was varied under the same precipitation condition to get a molar ratio of EDTA/Tb of 0, 0.5, 1.0, and 2.5. As shown in Fig. 5a, it is visible that no aggregate was formed in the starting solution without EDTA. The resultant products were irregular nanoparticles. When the molar ratio of EDTA to Tb is in the range of 0.5∼1, non-spherical aggregates with a width about 220 nm and a length about 300 nm were obtained (Fig. 5b and c). With the molar ratio of EDTA to Tb increased, the size of the non-spherical aggregates would decrease. Fig. 5d shows that rice-grain like aggregates with widths of about 70 nm and lengths of about 180 nm (a few were 130 nm in width and 220 nm in length) were formed in the solution with a molar ratio of EDTA/Tb at 2.5. In the present system, the molar ratio of EDTA/Tb is undoubtedly vital in the morphologies and self-assembly of $NaTbF_4$ nanostructures.

On the basis of the above experimental results, we propose that the Ostwald ripening process is involved in the formation mechanism of the novel mesoporous nano-rice (Scheme 1). It is known that EDTA is a strong chelator for rare earth ions and can form stable complexes with Ln^{3+} ions through coordination interaction. When EDTA was introduced, it can react with the Tb^{3+} ion to form the intermediate complex of Tb-EDTA (1 : 1), greatly decreasing the free Tb^{3+} ion concentration in the solution. Such a low Tb^{3+} ion concentration leads to a relatively slow reaction rate and facilitates the oriented growth of $NaTbF_4$ nanocrystals in the view of the dynamic process. When Tb-EDTA is attacked by F^-, the active {0001} facet of hexagonal

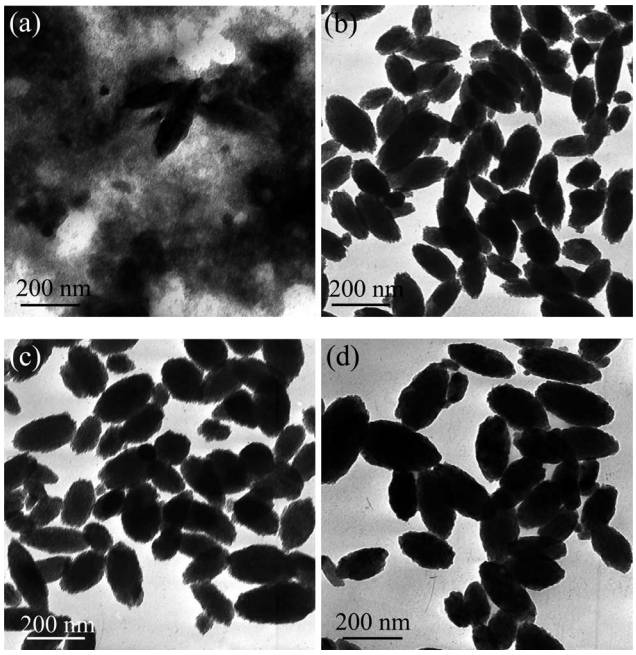

Fig. 4 TEM images of $NaTbF_4$ samples obtained by the reaction of Tb^{3+} with NaF in the presence of EDTA at 110 °C for (a) 0.5 h, (b) 1 h, (c) 2 h and (d) 6 h.

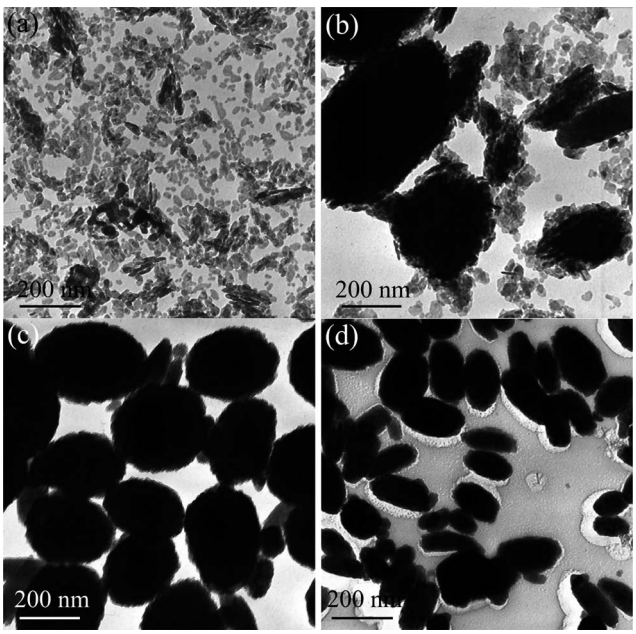

Fig. 5 TEM images of $NaTbF_4$ samples obtained in the solution with a molar ratio of EDTA to Tb at (a) 0, (b) 0.5, (c) 1 and (d) 2.5.

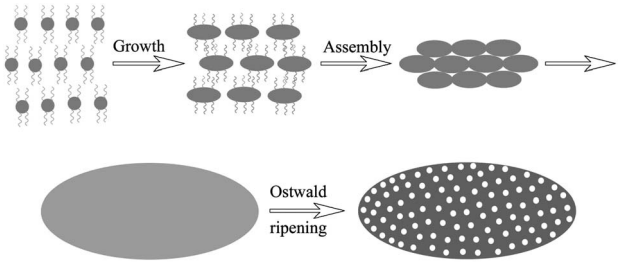

Scheme 1 Schematic illustration of the formation process of mesoporous $NaTbF_4$ nano-rice.

$NaTbF_4$ is restricted by the released EDTA ions. Thus the crystal growth along [0001] direction is confined, and it grows preferentially along [$\bar{2}$110] directions. This kinetic control leads to the formation of the original nanocrystals with the preferential growth directions. This hypothesis was confirmed by the infrared (IR) spectrum (see Fig. S2, ESI†), SAED pattern and HRTEM results. Subsequently, these nanocrystals assemble in layer-by-layer stacking style due to the hydrogen bonding and electrostatic effects of EDTA ions. Then rice-grain like aggregates, with intrinsic size/density variations inside, were formed with the help of the EDTA. Meanwhile, the aggregated nanocrystals underwent the Ostwald ripening process at the cost of the smaller nanoparticles, and mesopores are gradually generated within the nano-rice. So, it can be concluded that EDTA plays a double role in the reaction. One is to serve as the chelating ligand to form a stable complex with Tb^{3+} and further kinetically control the reaction rate; the other is to act as the capping agent to affect the facet growth and their assembly.

Eu^{3+} has a very close ion radius with Tb^{3+}, thus making it convenient to dope mesoporous $NaTbF_4$ nano-rice with designated amount of Eu^{3+}, which may then endow the mesoporous nano-rice with novel properties. To validate this hypothesis, we prepared a series of Eu-doped $NaTbF_4$ products under the same conditions *via* employing the mixture of Tb_2O_3 and Eu_2O_3 with a designated mole ratio as the precursor instead of pure Tb_2O_3. The morphologies and composition of the products were characterized by TEM, SEM, EDX and XRD (Fig. 6; Fig. S3–S5, ESI†). It is observed that, with increasing the Eu doping concentration to 2∼95%, the shape and size of the products remain almost unchanged. Also, the positions of the peaks of Eu-doped $NaTbF_4$ samples remain almost unchanged as well, indicating that Eu^{3+} has been incorporated into the $NaTbF_4$ lattice successfully.

In order to study the effect of the porous structure on the photoluminescence properties of the material, the emission spectra and luminescent dynamics were recorded on the solid samples of $NaTbF_4$:Eu (0∼95%) at room temperature. Fig. 7 shows the emission spectra of mesoporous $NaTbF_4$:Eu nano-rice with doping levels varying from 0 to 95% under 377 nm excitation. In the un-doped $NaTbF_4$ nano-rice, the characteristic emissions of Tb^{3+} are observed, which originate from the transitions from the excited $^5D_4$ to the ground states ^7F_j ($j = 6, 5, 4, 3$). With doping of Eu^{3+} (2∼95%), the obtained emission spectra exhibit characteristic lines of Eu^{3+}, and no emission from Tb^{3+} is observed, indicating that an efficient energy transfer occurs from Tb^{3+} to Eu^{3+} in the $NaTbF_4$:Eu nano-rice. Although the luminescent

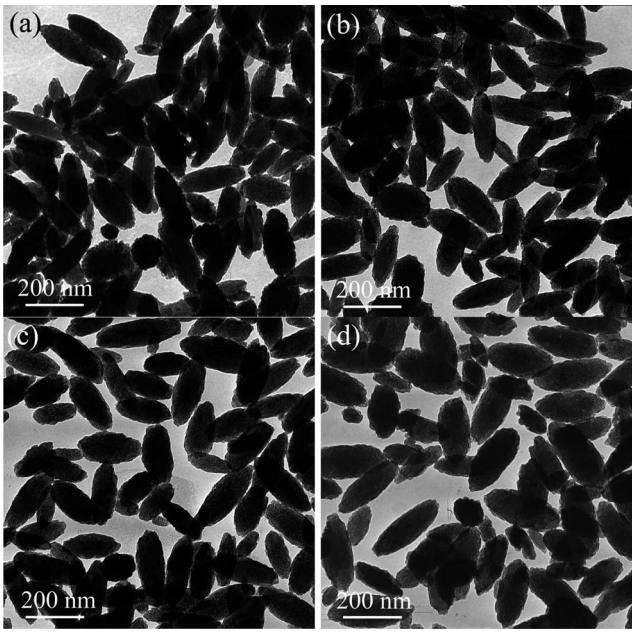

Fig. 6 TEM images of mesoporous $NaTbF_4$:Eu nano-rice doped with various amounts of Eu^{3+}: 95, 25, 10, and 2%, which were obtained in the solution with the molar ratio of Tb^{3+} to Eu^{3+} at (a) 1/19, (b) 3/1, (c) 9/1 and (d) 49/1, respectively.

positions of these $NaTbF_4$:Eu samples are identical, the luminescent intensity is much different. The luminescent intensity of low Eu^{3+} concentration samples is much higher than that of high Eu^{3+} concentration samples under the same measurement conditions. Generally, the increase of Eu^{3+} concentration enhances the probability of energy transfer from Tb^{3+} to Eu^{3+}. Meanwhile, the increase of Eu^{3+} concentration also increases the probability of non-radiative energy migration between Eu^{3+} ions to quenching centers, where the excitation energy is lost non-radiatively.[63] This is also confirmed by the luminescent dynamics of the $^5D_0$ state of Eu^{3+} in $NaTbF_4$:Eu nano-rice. As shown in Fig. 8, bi-exponential decays are observed. The decay components are (τ_1) 2.19 ms (96.7%) and (τ_2) 0.63 ms (3.3%), and the average decay time is 2.14 ms for the $NaTbF_4$:Eu (95%) sample. Similarly decay components

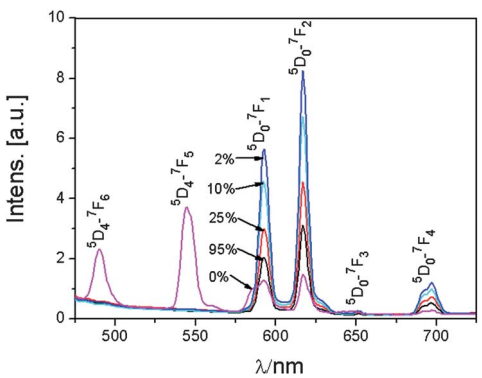

Fig. 7 Emission spectra of mesoporous $NaTbF_4$ nano-rice and those doped with various amounts of Eu^{3+}: 2, 10, 25, and 95% (λ_{ex} = 377 nm). The doping fraction was calculated on the basis of the molar ratio of Tb to Eu in the precursor mixture.

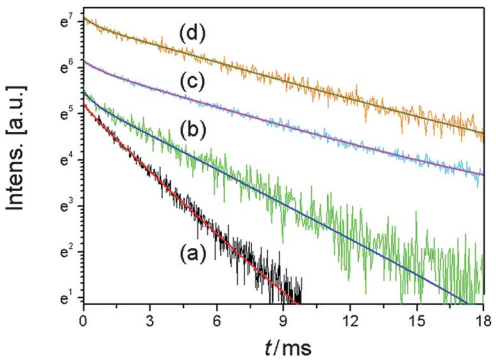

Fig. 8 The typical luminescent decay curves monitored at 592 nm for $NaTbF_4$:Eu mesoporous nano-rice containing (a) 95% Eu^{3+}, (b) 25% Eu^{3+}, (c) 10% Eu^{3+} and (d) 2% Eu^{3+} ($\lambda_{ex} = 377$ nm).

are (τ_1) 4.02 ms (92.6%) and (τ_2) 0.45 ms (7.4%), and the average decay time is 3.76 ms for the $NaTbF_4$:Eu (25%) sample. For the low Eu^{3+} concentration samples, a significant increase in the luminescence lifetimes is observed. The decay components are (τ_1) 6.75 ms (98.1%) and (τ_2) 0.73 ms (1.9%), and the average decay time is 6.64 ms for the $NaTbF_4$:Eu (10%) sample. The decay components are (τ_1) 7.06 ms (98.6%) and (τ_2) 0.51 ms (1.4%), and the average decay time is 6.97 ms for the $NaTbF_4$:Eu (2%) sample. The increase in the luminescence lifetimes indicates that the non-radiative energy migration between Eu^{3+} ions to quenching centers decreased in the low Eu^{3+} concentration samples.

On the basis of the emission spectra and lifetimes of the $^5D_0$ emitting level, the emission quantum efficiency (η) of Eu^{3+} excited state can be determined. Since the magnetic dipole of the $^5D_0 \rightarrow {}^7F_1$ transition is relatively intense to the chemical environments around the Eu^{3+} ion, it can be considered as a reference for the whole spectrum.[64,65] Radiative (A_{rad}), non-radiative (A_{nrad}) transitions, and average decay time are related through the following equation:[66,67]

$$A_{tot} = A_{rad} + A_{nrad} = \frac{1}{\tau} \quad (1)$$

where A_{rad} can be obtained by summing over the radiative rates A_{0j} for each $^5D_0 \rightarrow {}^7F_j$

$$A_{rad} = A_{01}\frac{\nu_{01}}{I_{01}}\sum_{J=0}^{4}\frac{I_{0j}}{\nu_{0j}} = \sum_{J} A_{0J} \quad (2)$$

where ν_{01} and ν_{0j} are the energy baricenters of the $^5D_0 \rightarrow {}^7F_1$ and $^5D_0 \rightarrow {}^7F_j$ transitions, respectively.[64] A_{01} is the Einstein's coefficient between $^5D_0 \rightarrow {}^7F_1$ and it is calculated using $A_{01} = n^3(A_{0-1})_{vac}$ where n is the average refractive index of the sample (1.341 for $NaTbF_4$ nano-rice) and $(A_{0-1})_{vac} = 14.65\ s^{-1}$. As quantum efficiency is expressed as the ratio between the number of photons emitted by Eu^{3+} ion and it is a balance between radiative and non-radiative process, η can be express as:

$$\eta = \frac{A_{rad}}{A_{rad} + A_{nrad}} \quad (3)$$

When eqn. 1–3 are applied, the parameters A_{rad}, A_{nrad} and η, for the $^5D_0$ Eu^{3+} ion excited state in the four mesoporous $NaTbF_4$:Eu samples can be obtained. As shown in Table 1, it can be seen that the emission quantum efficiency (η) decreases with increasing the Eu^{3+} concentration. This may be due to the concentration quenching effect. It is understandable that the concentration quenching effect is due to the possible non-radiative transfer between neighboring Eu^{3+} ions, which increases the mobility of the excited state within the host matrix and therefore increases the probability of non-radiative de-excitation *via* quenching centers. In the low Eu^{3+} concentration case, the emission quantum efficiencies of $NaTb_{0.9}Eu_{0.1}F_4$ and $NaTb_{0.98}Eu_{0.02}F_4$ samples are as high as 66.9% and 69.9%, respectively, indicating that the novel mesoporous $NaTbF_4$ nano-rice is an ideal host lattice for optically active lanthanide ions.

Table 1 Luminescent date of $NaTbF_4$:Eu (95%, 25%, 10% and 2%) samples

	$NaTbF_4$:Eu (95%)	$NaTbF_4$:Eu (25%)	$NaTbF_4$:Eu (10%)	$NaTbF_4$:Eu (2%)
ν_{01} (cm^{-1})	16 877	16 864	16 889	16 866
ν_{02} (cm^{-1})	16 208	16 208	16 206	16 208
ν_{03} (cm^{-1})	15 351	15 361	15 351	15 349
ν_{04} (cm^{-1})	14 348	14 346	14 348	14 346
τ (ms)	2.14	3.76	6.64	6.97
$1/\tau$ (ms)	0.467	0.266	0.151	0.143
A_{rad} (ms^{-1})	0.102	0.099	0.101	0.100
A_{nrad} (ms^{-1})	0.167	0.050	0.043	
η (%)	21.8	37.2	66.9	69.9

Conclusions

In conclusion, mesoporous $NaTbF_4$ and $NaTbF_4$:Eu rice-grain like architectures have been successfully synthesized *via* a simple complexing-agent-assisted hydrothermal approach. A series of characterizations confirmed the single-crystalline and mesoporous structured nature of the $NaTbF_4$ nano-rice. The experimental results indicate that EDTA plays an important role in the formation of the rice-grain like architectures. The formation and evolution of $NaTbF_4$ rice-grain like architectures was investigated and a possible mechanism was proposed to explain its formation. The optical properties of mesoporous $NaTbF_4$:Eu nano-rice are relevant to their doped-Eu^{3+} concentration. In the low Eu^{3+} concentration specimens, the maximum quantum efficiency of the Eu^{3+} excited state reaches up to 69.9%. Mesoporous structures and the special optical properties will endow the novel materials with promising applications in desorption, catalysis, optics, mass spectrometry detection, and biolabels.

Experimental

All the chemicals and reagents were of analytical grade, purchased from Sinopharm Chemical Reagent Co., Ltd. (Shanghai, China), and used without further purification. Deionized water was used throughout. In a typical synthesis, EDTA solution was obtained by dissolving 500 mg EDTA in 6.5 ml of 1 M sodium hydroxide solution. Sodium fluoride solution was obtained by dissolving 227 mg sodium fluoride in 7 ml water/ethanol (2/5, vol/vol). Tb_2O_3 (0.5 mmol) was completely dissolved in 6.8 ml of 0.74 M HNO_3 to form the $Tb(NO)_3$ solution. Then, the EDTA solution and 10 ml ethanol were added to the obtained $Tb(NO)_3$ solution in sequence. After 5 min in an ultrasonic bath, the NaF solution was introduced.

Subsequently, the mixed system was sonolyzed for 5 min to ensure homogeneous dispersion of all reagents in the solutions and transferred into a Teflon-lined autoclave. After the autoclave was tightly sealed and heated at 110 °C for 12 h, the system was allowed to cool to room temperature naturally. The as-obtained white precipitate was collected, washed with distilled water and absolute ethanol several times, and finally dried at 110 °C in air for 0.5 h. About 248 mg mesoporous $NaTbF_4$ nano-rice could be obtained. Using the same procedures, the concentration of EDTA, time scale, and the composition of metal precursors were varied in the experiments to obtain products with a desired morphology and composition.

X-ray diffraction (XRD) patterns of the products were recorded on a Shimadzu XRD-6000 X-ray diffractometer with Cu-Kα radiation ($\lambda = 0.15406$ nm) at a scanning rate of 0.1 °s^{-1} in the 2θ range from 20 to 80°. Transmission electron microscopy (TEM) images were obtained on a JEM-200CX transmission electron microscope, with an accelerating voltage of 200 kV. Energy dispersive X-ray (EDX) analysis and scanning electron microscopy (SEM) images were taken on a Hitachi S-4800 scanning electron microscope with an energy-dispersive X-ray spectroscope. High-resolution TEM (HRTEM) images were acquired from a JEM 2010 high-resolution transmission electron microscope. The nitrogen sorption isotherms and the Barrett–Joyner–Halenda (BJH) pore size distribution curve of the samples were obtained using the micropore program with a Micromeritics ASAP2020 instrument, after de-gassing the samples *in situ* at 300 °C for 4 h. Fourier transform infrared spectrum (FT-IR) was obtained on a Vectortm 22. We pressed the nano-rices to form a smooth, opaque flat disk for optical study. Spectroscopic ellipsometry measurements were made using a Sopra GES-5E spectroscopic ellipsometer in a typical wavelength range of 300–800 nm at angle of incidence 75° to obtain ellipsometric angles. The experimental data were fitted using a classical Lorentz oscillator model to calculate the refractive index of $NaTbF_4$ nano-rice. Luminescent spectra were carried out on an Aminco Bowman luminescence spectrometer equipped with a 150 W Xe arc lamp at room temperature. The luminescence lifetime of Eu^{3+} was measured using an Edinburgh Instruments' FLS 920 instrument with a Pulsed Xenon Micro-second Flash Lamp (μF900) and a red sensitive R928-P (185∼870 nm). All lifetime analyses were calculated using the Edinburgh Instruments F900 software and signal intensities greater than 1% of the maximum intensity were included, and were fitted so as to obtain χ^2 values from 1.0 to 1.3.

Acknowledgements

This work was supported by the National Natural Science Foundation of China (21075064, 21027013, 21021062, and 90813020) and the National Basic Research Program of China (2007CB925102).

References

1 C. X. Li, J. Yang, P. P. Yang, H. Z. Lian and J. Lin, *Chem. Mater.*, 2008, **20**, 4317–4326.
2 Y. N. Xia, P. D. Yang, Y. G. Sun, Y. Y. Wu, B. Mayers, B. Gates, Y. D. Yin, F. Kim and H. Q. Yan, *Adv. Mater.*, 2003, **15**, 353–389.
3 X. Y. Kong, Y. Ding, R. Yang and Z. L. Wang, *Science*, 2004, **303**, 1348–1351.
4 Y. Wang, H. R. Li, Y. Feng, H. J. Zhang, G. Calzaferri and T. Z. Ren, *Angew. Chem. Int. Ed.*, 2010, **49**, 1434–1438.
5 Y. Ding, S. H. Yu, C. Liu and Z. A. Zang, *Chem.–Eur. J.*, 2007, **13**, 746–753.
6 F. Jiao, A. Harrison, J. C. Jumas, A. V. Chadwick, W. Kockelmann and P. G. Bruce, *J. Am. Chem. Soc.*, 2006, **128**, 5468–5474.
7 X. W. Lou, Y. Wang, C. L. Yuan, J. Y. Lee and L. A. Archer, *Adv. Mater.*, 2006, **18**, 2325–2329.
8 B. Liu and H. C. Zeng, *Small*, 2005, **1**, 566–571.
9 X. X. Yu, J. G. Yu, B. Cheng and B. B. Huang, *Chem.–Eur. J.*, 2009, **15**, 6731–6739.
10 Y. W. Tan, S. Srinivasan and K. S. Choi, *J. Am. Chem. Soc.*, 2005, **127**, 3596–3604.
11 F. Zhang, Y. F. Shi, X. H. Sun, D. Y. Zhao and G. D. Stucky, *Chem. Mater.*, 2009, **21**, 5237–5243.
12 W. Feng, L. D. Sun, Y. W. Zhang and C. H. Yan, *Small*, 2009, **5**, 2057–2060.
13 X. Wang and Y. D. Li, *Angew. Chem., Int. Ed.*, 2003, **42**, 3497–3500.
14 Y. Li, M. H. Cao and L. Y. Feng, *Langmuir*, 2009, **25**, 1705–1712.
15 W. S. Choi, H. Y. Koo, Z. Zhongbin, Y. D. Li and D. Y. Kim, *Adv. Funct. Mater.*, 2007, **17**, 1743–1749.
16 D. Y. Zhao, J. L. Feng, Q. S. Huo, N. Melosh, G. H. Fredrickson, B. F. Chmelka and G. D. Stucky, *Science*, 1998, **279**, 548–552.
17 P. D. Yang, T. Deng, D. Y. Zhao, P. Y. Feng, D. Pine, B. F. Chmelka, G. M. Whitesides and G. D. Stucky, *Science*, 1998, **282**, 2244–2246.
18 S. Schacht, Q. Huo, I. G. Voigt-Martin, G. D. Stucky and F. Schüth, *Science*, 1996, **273**, 768–771.
19 P. Schmidt-Winkel, W. W. Lukens, P. D. Yang, D. I. Margolese, J. S. Lettow, J. Y. Ying and G. D. Stucky, *Chem. Mater.*, 2000, **12**, 686–696.
20 U. Ciesla, M. Fröba, G. D. Stucky and F. Schüth, *Chem. Mater.*, 1999, **11**, 227–234.
21 Y. Y. Wu, T. Livneh, Y. X. Zhang, G. S. Cheng, J. F. Wang, J. Tang, M. Moskovits and G. D. Stucky, *Nano Lett.*, 2004, **4**, 2337–2342.
22 P. D. Yang, A. H. Rizvi, B. Messer, B. F. Chmelka, G. M. Whitesides and G. D. Stucky, *Adv. Mater.*, 2001, **13**, 427–431.
23 P. Schmidt-Winkel, C. J. Glinka and G. D. Stucky, *Langmuir*, 2000, **16**, 356–361.
24 Q. H. Shi, H. J. Liang, D. Feng, J. F. Wang and G. D. Stucky, *J. Am. Chem. Soc.*, 2008, **130**, 5034–5035.
25 X. H. Sun, Y. F. Shi, P. Zhang, C. M. Zheng, X. Y. Zheng, F. Zhang, Y. C. Zhang, N. J. Guan, D. Y. Zhao and G. D. Stucky, *J. Am. Chem. Soc.*, 2011, **133**, 14542–14545.
26 Y. Wan and D. Y. Zhao, *Chem. Rev.*, 2007, **107**, 2821–2860.
27 Y. Wan and D. Y. Zhao, *Acc. Chem. Res.*, 2006, **39**, 423–432.
28 Y. Wan, Y. F. Shi and D. Y. Zhao, *Chem. Mater.*, 2008, **20**, 932–945.
29 C. Dickinson, W. Z. Zhou, R. P. Hodgkins, Y. F. Shi, D. Y. Zhao and H. Y. He, *Chem. Mater.*, 2006, **18**, 3088–3095.
30 Y. H. Deng, C. Liu, T. Yu, F. Liu, F. Q. Zhang, Y. Wan, L. J. Zhang, C. C. Wang, B. Tu, P. A. Webley, H. T. Wang and D. Y. Zhao, *Chem. Mater.*, 2007, **19**, 3271–3277.
31 Y. F. Shi, Y. Wan, Y. P. Zhai, R. L. Liu, Y. Meng, B. Tu and D. Y. Zhao, *Chem. Mater.*, 2007, **19**, 1761–1771.
32 N. K. Raman, M. T. Anderson and C. J. Brinker, *Chem. Mater.*, 1996, **8**, 1682–1701.
33 D. A. Doshi, A. Gibaud, V. Goletto, M. C. Lu, H. Gerung, B. Ocko, S. M. Han and C. J. Brinker, *J. Am. Chem. Soc.*, 2003, **125**, 11646–11655.
34 C. J. Brinker and D. R. Dunphy, *Curr. Opin. Colloid Interface Sci.*, 2006, **11**, 126–132.
35 Y. Yamauchi and K. Kuroda, *Chem.–Asian J.*, 2008, **3**, 664–676.
36 T. Kimura, Y. Sugahara and K. Kuroda, *Microporous Mesoporous Mater.*, 1998, **22**, 115–126.
37 M. Sakurai, A. Shimojima, M. Heishi and K. Kuroda, *Langmuir*, 2007, **23**, 10788–10792.
38 G. S. Zhu, S. L. Qiu, F. F. Gao, D. S. Li, Y. F. Li, R. W. Wang, B. Gao, B. S. Li, Y. H. Guo, R. R. Xu, Z. Liu and O. Terasaki, *J. Mater. Chem.*, 2001, **11**, 1687–1693.
39 M. Inagaki, T. Morishita, T. A.KunoKito, M. Hirano, T. Suwa and K. Kusakawa, *Carbon*, 2004, **42**, 497–502.
40 S. Fujita, H. Nakano, M. Ishii, H. Nakamura and S. Inagaki, *Microporous Mesoporous Mater.*, 2006, **96**, 205–209.

41 Y. S. Tao, M. Endo, M. Inagaki and K. Kaneko, *J. Mater. Chem.*, 2011, **21**, 313–323.
42 X. Wang, J. Zhuang, Q. Peng and Y. D. Li, *Inorg. Chem.*, 2006, **45**, 6661–6665.
43 S. Heer, O. Lehmann, M. Haase and H. U. Gudel, *Angew. Chem., Int. Ed.*, 2003, **42**, 3179–3182.
44 J. W. Stouwdam and F. C. J. M. van Veggel, *Nano Lett.*, 2002, **2**, 733–737.
45 Z. M. Chen, Z. R. Geng, D. L. Shao, Y. H. Mei and Z. L. Wang, *Anal. Chem.*, 2009, **81**, 7625–7631.
46 G. S. Yi, H. C. Lu, S. Y. Zhao, Y. Ge, W. J. Yang, D. P. Chen and L. H. Guo, *Nano Lett.*, 2004, **4**, 2191–2196.
47 H. C. Lu, G. S. Yi, S. Y. Zhao, D. P. Chen, L. H. Guo and J. Cheng, *J. Mater. Chem.*, 2004, **14**, 1336–1341.
48 S. Sivakumar, P. R. Diamente and F. C. J. M. van Veggel, *Chem.–Eur. J.*, 2006, **12**, 5878–5884.
49 L. Y. Wang, R. X. Yan, Z. Y. Huo, L. Wang, J. H. Zeng, J. Bao, X. Wang, Q. Peng and Y. D. Li, *Angew. Chem., Int. Ed.*, 2005, **44**, 6054–6057.
50 K. B. Zhou, X. Wang, X. M. Sun, Q. Peng and Y. D. Li, *J. Catal.*, 2005, **229**, 206–212.
51 H. Maas, A. Currao and G. Calzaferri, *Angew. Chem., Int. Ed.*, 2002, **41**, 2495–2496.
52 X. Wang and Y. D. Li, *Chem.–Eur. J.*, 2003, **9**, 5627–5635.
53 R. X. Yan and Y. D. Li, *Adv. Funct. Mater.*, 2005, **15**, 763–770.
54 M. M. Lezhnina, T. Jüstel, H. Kätker, D. U. Wiechert and U. H. Kynast, *Adv. Funct. Mater.*, 2006, **16**, 935–942.
55 F. Zhang, J. Li, J. Shan, L. Xu and D. Y. Zhao, *Chem.–Eur. J.*, 2009, **15**, 11010–11019.
56 M. Yada, M. Mihara, S. Mouri, M. Kuroki and T. Kijima, *Adv. Mater.*, 2002, **14**, 309–313.
57 K. L. Frindell, M. H. Bartl, A. Popitsch and G. D. Stucky, *Angew. Chem., Int. Ed.*, 2002, **41**, 959–962.
58 D. V. Bavykin, V. N. Parmon, A. A. Lapkin and F. C. Walsh, *J. Mater. Chem.*, 2004, **14**, 3370–3377.
59 K. S. W. Sing, D. H. Everett, R. A. W. Haul, L. Moscou, R. A. Pierotti, J. Rouquerol and T. Siemieniewska, *Pure Appl. Chem.*, 1985, **57**, 603–619.
60 J. H. Zeng, Z. H. Li, J. Su, L. Y. Wang, R. X. Yan and Y. D. Li, *Nanotechnology*, 2006, **17**, 3549–3555.
61 Z. M. Chen, Z. R. Geng, M. L. Shi, Z. H. Liu and Z. L. Wang, *CrystEngComm*, 2009, **11**, 1591–1596.
62 Z. M. Chen, Z. R. Geng, Z. Y. Zhang, Z. H. Liu and Z. L. Wang, *CrystEngComm*, 2010, **12**, 2841–2846.
63 A. Huignard, T. Gacoin and J. P. Boilot, *Chem. Mater.*, 2000, **12**, 1090–1094.
64 C. Y. Peng, H. J. Zhang, J. B. Yu, Q. G. Meng, L. S. Fu, H. R. Li, L. N. Sun and X. M. Guo, *J. Phys. Chem. B*, 2005, **109**, 15278–15287.
65 L. Zhu, X. M. Liu, J. Meng and X. Q. Cao, *Cryst. Growth Des.*, 2007, **7**, 2505–2511.
66 A. Kar and A. Patra, *J. Phys. Chem. C*, 2009, **113**, 4375–4380.
67 A. Kar, A. Datta and A. Patra, *J. Mater. Chem.*, 2010, **20**, 916–922.